Spray-drying-derived amorphous calcium phosphate: a multi-scale characterization

Sylvain Le Grill, Jérémy Soulié, Yannick Coppel, Pierre Roblin, Pierre Lecante, Olivier Marsan, Cédric Charvillat, Ghislaine Bertrand, Christian Rey, Fabien Brouillet

Spray-drying-derived amorphous calcium phosphate: a multi-scale characterization

Sylvain Le Grill[1], Jeremy Soulie[1], Yannick Coppel[2], Pierre Roblin[3], Pierre Lecante[4], Olivier Marsan[1], Cédric Charvillat[1], Ghislaine Bertrand[1], Christian Rey[1], and Fabien Brouillet[1,*]

[1]CIRIMAT, Université de Toulouse, CNRS, INP- ENSIACET, Université de Toulouse, 4 allée Emile Monso, 31030 Toulouse, France
[2]LCC, UPR 8241 CNRS, Université de Toulouse, 205 route de Narbonne, Toulouse, France
[3]LGC, CNRS, Université de Toulouse, 118 route de Narbonne Bâtiment 2R1, Toulouse, France
[4]CEMES, CNRS, Université de Toulouse, 29 Rue Jeanne Marvig, Toulouse, France

ABSTRACT

Amorphous calcium orthophosphates (ACP) are bioactive compounds presenting high interest as bone substitute. However, the synthesis of such metastable products requires special attention as they can rapidly evolve into a crystalline phase during the elaboration process. The resulting increased stability generally leads to less bioactive reactive materials. Among the various strategies developed to obtain stable form of ACP, the use of spray drying is an effective and reproducible route. Compared to previous works, this study aims to demonstrate for the first time the feasibility of ACP elaboration by spray drying directly from a single solution of selected precursors. Moreover, structuration of the spray-dried powders was determined at different length scales, demonstrating a hierarchical organization from nanometric clusters to particles aggregates. These complementary analyses highlighted a thorough mechanism of particles formation during processing. The effect of the initial composition of the solution was observed, and it was demonstrated that there is a correlation with the purity of the final product that may be modulated. In addition, ACP powders were found to be highly reactive in aqueous medium and their fast transformation into low crystalline apatite suggests a good suitability for biomedical use.

Introduction

Amorphous calcium orthophosphates (ACPs) are a family of metastable mineral compounds involved in the formation of several calcium phosphate phases. In particular, they are known as in vitro [1–3] and in vivo [4–6] precursors of apatite like phase, the mineral phase of hard tissues of vertebrates and one of the major orthopedic biomaterials. Due to their high solubility and reactivity, ACPs appear to be promising compounds for resorbable bone substitution/regeneration applications. In addition, some ACPs have even been shown to present a high osteoinductivity [7] favoring bone neo-formation within the implant. ACPs can be used for instance as solid precursors in bone substitute calcium phosphate cements [8, 9] or in dental pastes [10] because of their ability to dissolve and release calcium and phosphate ions for dentin and enamel remineralization.

The main route to produce synthetic ACPs is based on the double decomposition between calcium and phosphate salts in aqueous media. It is well established that the resulting ACPs are a multi-scale material [11]. Indeed, ACPs spontaneously precipitate into 1-nm clusters grouped in spherical nanoparticles [12] that are organized themselves in chain-like structure [11]. Currently, one of the common morphology and composition description of the ACP building units is based on the Posner's cluster [13]. This model has been developed comparing pair distribution functions (PDF) of ACP and hydroxyapatite (HAp). In short distances, great similarities were found in the positions of P–O, O–O and Ca–O, Ca–Ca and P–P ions pairs, but a peak cut-off was observed in the ACP PDF at about 1 nm. Posner's clusters are then 1-nm spherical particles with the $Ca_9(PO_4)_3$ formula (cluster existing in the core of HAp crystal [14] and theoretically anhydrous). This formula with Ca/P ratio of 1.5 is the only one possible for ACP containing only PO_4^{3-} anions and Ca^{2+} cations. However, even though the shape and size of this amorphous cluster are regularly confirmed, the Ca/P ratio of ACPs may depart from its theoretical value 1.5 and is reported in a range from 1.18 to 2. For values under 1.5 with samples containing only orthophosphate and calcium ions, the observed Ca/P values correspond to the existence of HPO_4^{2-} species and the correlative decrease of positive Ca^{2+} ions to maintain the electroneutrality. The hydrogenophosphate amount depends on the pH of the precipitation solution or post-treatment (for example washing, or ageing) [15, 16]. For samples with a Ca/P ratio above 1.5, with an excess of calcium ions, foreign anions are necessary to maintain the electroneutrality, most generally carbonates [17]. In addition, ACPs are prone to incorporate many impurities or additives counter ions from synthesis solutions, including ions of biological interest like Mg^{2+}, Zn^{2+} and Sr^{2+}.

Elaboration and stabilization of synthetic ACPs are challenging as the spontaneous evolution of these metastable phases toward a more stable, crystalline phase most generally apatite, needs to be controlled. Several strategies have been proposed. The one most common is partly inspired by in vivo observations and based on the growth inhibition of apatite by adding various amounts of ionic additives [16]. For example, the presence of carbonate [18], magnesium, strontium [19], or pyrophosphates [20] ions was found to slow down crystallization and/or to stabilize the amorphous phase.

The second way is based on a control of process parameters like temperature or contact time with reagents in solution. Ortali et al. [21] showed that the crystallization state of calcium phosphate precipitates varies according to the temperature and that well crystallized HAp, poorly crystallized apatite and ACP can be obtained, respectively, at 90 °C, 60 °C and 37 °C. The same synthesis can also lead to either ACP or HAP depending on the addition rate of reactants and the mixing time in solution [22] before the separation of the precipitate by filtration, centrifugation, or settling. These steps have to be carefully controlled to prevent possible evolution of the non-thermodynamically stable phase and to finally obtain reproducible products. It shall be noted that the conversion of ACPs into apatite in wet media is considered as an autocatalytic reaction, the rate of which is determined by the amount of already formed apatite seeds [23]. In all cases, the conversions of ACPs to crystalline phases necessitate water, and thus drying appears as an essential step for ACPs preservation. Freeze-drying to evaporate residual water is often the preferred drying process.

An alternative way to stop the reaction and dry up the precipitate at the earliest stage of the process consists in using a dynamic drying method: spray drying which is a continuous operation that can be performed at high drying rates for direct production

of dried powder from a liquid preparation of temperature sensitive material. This technique was proposed to elaborate ACP by Chow et al., Xu et al. [24, 25] or Melo et al. [26]. In these studies, the authors firstly synthetized a crystalline calcium phosphate phase that is solubilized in an acidic medium before spray drying. The Ca/P ratio in the resulting ACP is then the same than that in the initial solubilized compound. Sun et al. [27] proposed in their study to elaborate ACP by spray drying using only calcium and phosphate precursors solutions. They used a basic calcium solution and an acidic phosphate solution. To prevent any anticipated precipitation, the two liquids were separated and a two-liquid nozzle allowing mixing just prior to spraying was used for the precipitation of ACP. The efficiency of this kind of nozzle may depend of the fine control during fast mixing of the solutions. This method has been reported to be a one-step (but not a one-pot) process to produce ACP with no post-treatment.

The aim of our study was to produce ACP powder by spray drying from a single solution of selected ionic precursors. We intended to use micro-droplets of the spray drier as micro-reactors for the precipitation of calcium phosphate using calcium acetate and phosphoric acid in a diluted solution. These calcium phosphate precursors were previously used by Safronova et al. [28] to produce ACP in batch. The resulting products expected for the precipitation reaction are an ACP powder and acetic acid which is a volatile compound more likely to be eliminated during the drying step. To the best of our knowledge, it is the first description of one-step and one-pot synthesis of ACP powder, supported by a fine multi-scale morphological analysis conducted in order to assess precipitation mechanism during spray drying. Two solutions with different Ca/P molar ratios were used (1.67 and 1.3), and a preliminary study of the resulting powder evolution in deionized water has been carried out in order to determine the reactivity and potential applications of the spray-dried powder.

Materials and methods

Phosphoric acid (H3PO4–PA–85%) and monohydrate calcium acetate ($Ca(CH3COO)_2 \cdot H2O$–CA) were purchased from Sigma-Aldrich. Two solutions of calcium phosphate precursors with Ca/P molar ratios of 1.3 and 1.67 were prepared by dissolving 5 g of CA in 1 L of deionized water and adding drop by drop under vigorous stirring 1.5 ± 0.05 and 1.2 ± 0.05 mL of PA, respectively. The ionic concentrations were established previously to avoid any homogeneous precipitation of calcium phosphate salts. Solutions were then spray-dried with a Mini Spray Dryer B 290 (BÜCHI, Switzerland) with an inset temperature of 160 °C, an air flow of 414 L/h, an aspiration of 90% and a liquid feed rate of 0.3 L/h. The resulting powders obtained with these solutions were, respectively, named **ACP 1.3** and **ACP 1.67**.

In order to consider a potential impact of the spray drying process on the chemical or crystallographic evolution of the precursor used in this study, a solution of 5 g of calcium acetate in 1 L deionized water has been spray-dried using the same conditions as in the present study. The resulting powder will be called **SDCA** (spray-dried calcium acetate).

Particle size distributions were investigated using a Mastersizer 3000 (Malvern) with an Aero S module (3 bars pressure, 10% obturation, 10 s accumulation) and averaged from three measurements. The evolution of the particle size of 2 g of powder in 100 mL of deionized water was recorded with a Hydro SM module (1500 rpm stirring, acquisition was recorded with 40% obturation and during 10 s every 30 s).

The morphology of the spray-dried powders was examined using scanning electron microscopy (SEM), and images were recorded in secondary electron mode (SE) with a LEO 435 VP, at a working distance of 10 mm and an accelerating voltage of 10 kV. Samples were previously set in position on a carbon adhesive band and metallized using a silver plasma during 3 min on a Scancoat 6 Sputter Coater.

For the TEM observations (recorded with a Jeol JEM-1400 under 80 kV acceleration), powders were dispersed in an epoxy resin at 60 °C for 48 h. These preparations were then dry cut (80 nm thickness) with an ultra-microtome and picked up on a copper grid.

A small-angle X-ray scattering (SAXS) using a XEUSS 2.0 device with a copper X-ray source was used at the wavelength λ = 1.5 Å. The powder was placed between two layers of Kapton® and was recorded at two distances (d = 387.5 mm and 1216.5 mm) in order to obtain a large q range starting from 0.004 to 1.5 Å-1 with a large interconnection region ranging from 0.03 to 0.5 Å-1. The data were recorded on detector Pilatus 1 M (Dectris), and the integration/reduction process of the 2D images was

performed with Foxtrot. To describe the behavior at the nanoscale, the following model computed with Sasview was implemented:

$$I(q) = I(q)_{PwLw} + I(q)_{BrdPeak} = Aq^{\ P} + \frac{B}{1 + \left(|q - q_0|\right)^m} \quad (1)$$

The first term corresponds to a power law function used to determine the surface state (value P) of large size object. The second term of the equation gives an empirical functional form for SAS data characterized by a broad scattering peak encountered in amorphous material, with a characteristic distance d ($d = 2\pi/q0$) between the scattering particles [29].

A prototype device dedicated to amorphous and nano-crystallized material was used for WAXS acquisition. A molybdenum source ($K\alpha$ = 0.71069 Å) was used at 50 kV and 20 mA. Recording time was typically 20 h. Samples were sealed inside Lindemann glass capillaries (1.5 mm in diameter). Pair distribution function (PDF) was obtained by Fourier transformation according to [30, 31].

X-ray diffraction was carried out with an INEL Equinox 1000 device with a Co anticathode ($K\alpha$ = 1.78897 Å) at 30 kV and 30 mA. The 10°–60° 2θ diffraction angle patterns were recorded during 1 h. A small diffraction peak at 22° 2θ due to the apparatus is observable when the diffraction intensity is too low.

A Bruker Avance III HD 400 (9.4 T) spectrometer was used for the NMR acquisition. References are tetramethylsilane for ^{1}H and ^{13}C and 85% phosphoric acid for the ^{31}P nuclei. $^{1}H/^{31}P$ double cross-polarization MAS ($^{1}H/^{31}P$ DCP MAS) $^{1}H \rightarrow {}^{31}P \rightarrow {}^{1}H$ were performed using 4-mm zircon rotors and 10 kHz rotations. This kind of experiment allows to probe the ^{1}H resonances close to ^{31}P nuclei in the calcium phosphate phase [32]. Two consecutive magnetization transfers from ^{1}H to ^{31}P and from ^{31}P to ^{1}H are done with respective contact times of $\tau 1$ = 1 ms and $\tau\tau$ of either 0.05 ms or 1 ms. Long time $\tau 2$ probes the further environment, while the short time probes the closest one. Three ^{31}P CP have been acquired with the sample ACP 1.3 in static mode and with three contact time of 0.05, 0.1 and 2 ms. All acquisitions were made at room temperature (21 °C).

FTIR spectroscopy (Nicolet 5700 Thermo) was used (400–4000 cm^{-1}) with a 2 cm^{-1} resolution in transmission mode. (Approximately 1 mg of powder was dispersed in 300 mg KBr, and a pellet was formed using an 8 T pressure for 30 s.) The ACP spectra were normalized with the 1078 cm^{-1} peak (stretching ν3 PO4 line).

Thermal gravimetric analysis and differential thermal analysis (TGA and DTA) were performed to characterize potential weight loss and potential crystallization with a Setsys evolution TGA (SETARAM instrumentation) in an alumina cup with a heat ramp of 5 °C/min from 25 to 1000 °C.

Evolution tests were carried out in deionized water. Typically, 1 g of dry powder was dispersed in 50 mL of water [33] and then freeze-dried at 2 min, 1, 4, 5, 7, 24 and 54 h. The pH of the solution was recorded during this experience and was allowed to evolve freely.

Results

SEM images of ACP 1.67 and ACP 1.3 (Fig. 1a, d, respectively) show that the powder resulting from the spray drying of a precursors solution has a micrometric size regardless of the Ca/P ratio characterized by a Volume Median Diameter of Dv50 = 2.2 and 2.4 μm, respectively. The micro-particles are more or less spherical in shape and looks like aggregates of smaller particles. The apparent porosity of these aggregates decreases when the Ca/P molar ratio increases. At the highest magnification, a multiscale organization appears. Indeed, SEM images (Fig. 1b, e, respectively, ACP 1.67 and ACP 1.3) revealed that micro-particles are themselves made of spherical nanoparticles of about 100 nm closely packed in a chain-like organization. TEM images (Fig. 1c, f) confirm the presence of these 100 nm particles and their chain-like organization also described by [12, 34]. This structure appears to be present both at the surface (i.e., the air/droplet interface during the spray drying) and in the core (i.e., the inner part of the droplet) of the dried particles. Spherical bubbles appearing in light grey on the images have been attributed to beam damages.

Equation (1) was applied to the SAXS data recorded on ACP 1.67 and ACP 1.3 as shown in Fig. 2. The SAXS plots at small angles are characterized by a large decay following a power law function with p = 4, indicating that the large clusters observed in microscopy present a defined surface. The second term of the equation allows us to describe the broad peak observed at intermediate angles, correlated with

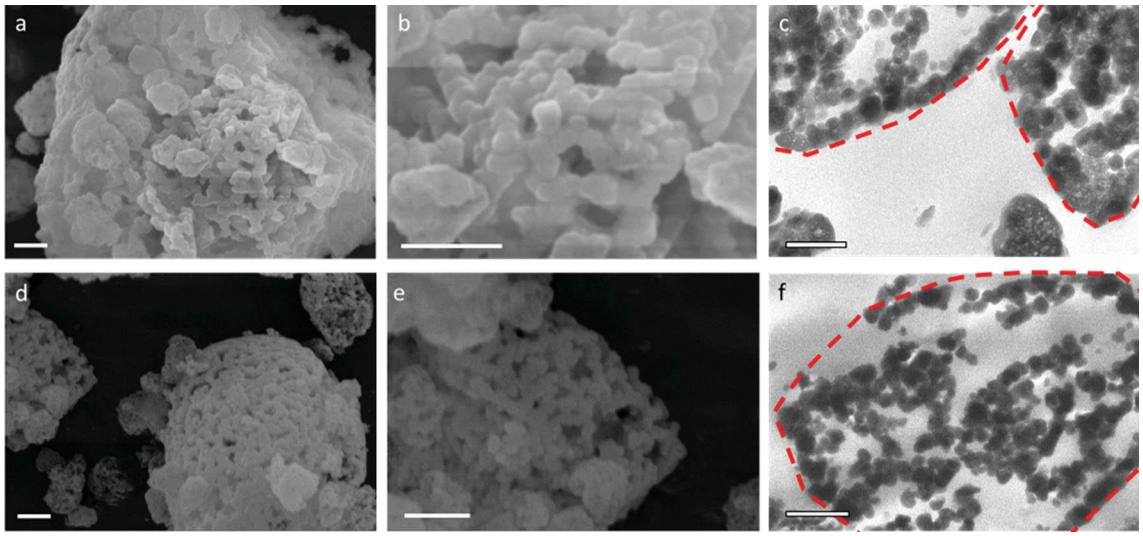

Figure 1 SEM (**a, b, d, e**) and TEM images of ACP 1.67 (**c**) and ACP 1.3 (**f**) Scale bar: 1 μm. The dot line represents the particle border.

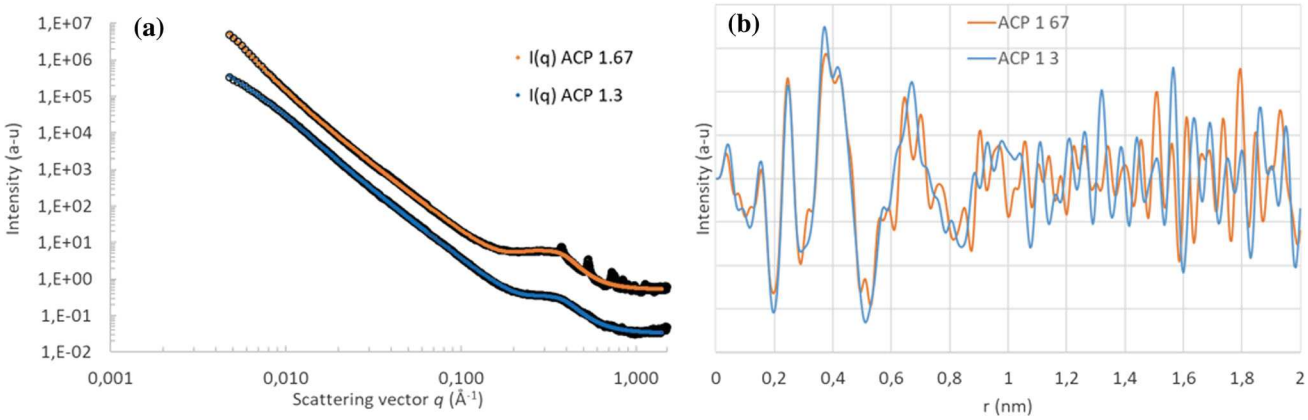

Figure 2 **a** SAXS data recorded on ACP 1.3 and 1.67 materials. The intensity is plotted as a function of Log($I(q)$) Log q in arbitrary units. The experimental curves are plotted in dark dots, and the corresponding fitting curves are plotted in blue dots for ACP 1.3 and in orange dots for ACP 1.67 and **b** WAXS PDF of ACP 1.67 and ACP 1.3.

the presence of short distance interactions between the smallest entities. Starting from the value of $q_0 = 0.32$ Å^{-1}, we estimated this d-spacing distance close to 2 nm and the volume fraction at 36% with the following relation $d = (\mathrm{Vol_{Fract}}/\mathrm{Vol_{part}})^{-1/3}$. No significant differences are observed between the both curves, except for the presence of diffraction peaks observed for the ACP 1.67 assigned to hemihydrated calcium acetate identified by X-ray diffraction (Fig. 3) [35]. We can notice that the broad peak is slightly more intense for ACP 1.67 reflecting a better interparticular arrangement.

To corroborate the analysis, a WAXS study has been carried out and the pair distribution functions of the materials are presented in Fig. 2b. The peaks at 1.6, 2.5, 3.7 and 4.2 Å can be attributed to P–O, Ca–O, Ca–P and P–P atomic pairs, respectively, with peak width like the one expected for an ACP cluster [13]. A cut-off of about 1 nm is observed in these PDF profiles regardless of the Ca/P ratio. Compared to the literature, this cut-off is less pronounced, due to the contribution of an additional organized calcium acetate phase (Figure S1, Supporting Information). This result is not in accordance with the center-to-center distance of 2 nm detected by SAXS, and this point will be discussed later. The contribution at $r < 1.6$ Å is characteristic of a covalent bond length, betraying the presence of another species, probably acetate, in the drying powder. If so, this species is in

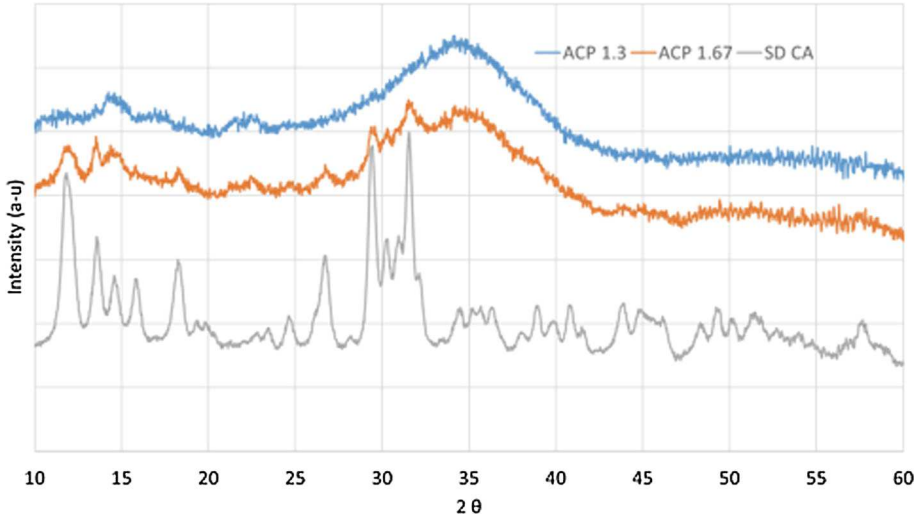

Figure 3 XRD pattern of the ACP 1.3, ACP 1.67 and SD CA powders. Each sharp peaks of SD CA correspond to the $Ca(CH_3COO)_2{\cdot}H_2O$(JCPDS 19–0199) except the diffraction peak at 22° 2θ that is due to an artifact to the apparatus. Beyond the wide halo centered around 35° 2θ and typical of an amorphous phase, some of these peaks (in particular 18.4, 29.3 and 31.5° 2θ) are detected for ACP 1.67 and to a less extent for the ACP 1.3.

low quantity as its contribution is minor in the *r* range.

Thermal analysis of the ACP 1.67 powder (Fig. 4) shows weight losses below 200 °C (13.5%), 400 °C (7.1%) and 800 °C (3%). Considering the reagents used in this study and according to literature [36], some calcium acetate is present in the final powder as a side product, explaining its high Ca/P ratio. The three main weight losses observed at increasing temperatures correspond then, respectively, to the departure of hydration water of the calcium acetate and the ACP (under 200 °C), and the second weight loss corresponds to two reactions reported in this range the condensation of HPO_4^{2-} into $P_2O_7^{4-}$ ions:

$$2\ HPO_4^{2-} \rightarrow P_2O_7^{4-} + H_2O \qquad \text{(reaction 1)}$$

and the decomposition of the calcium acetate moiety with a release of acetone and/or oxidation products:

$$Ca(CH_3COO)_2 \rightarrow (CH_3)_2CO + CaCO_3 \qquad \text{(reaction 2)}$$

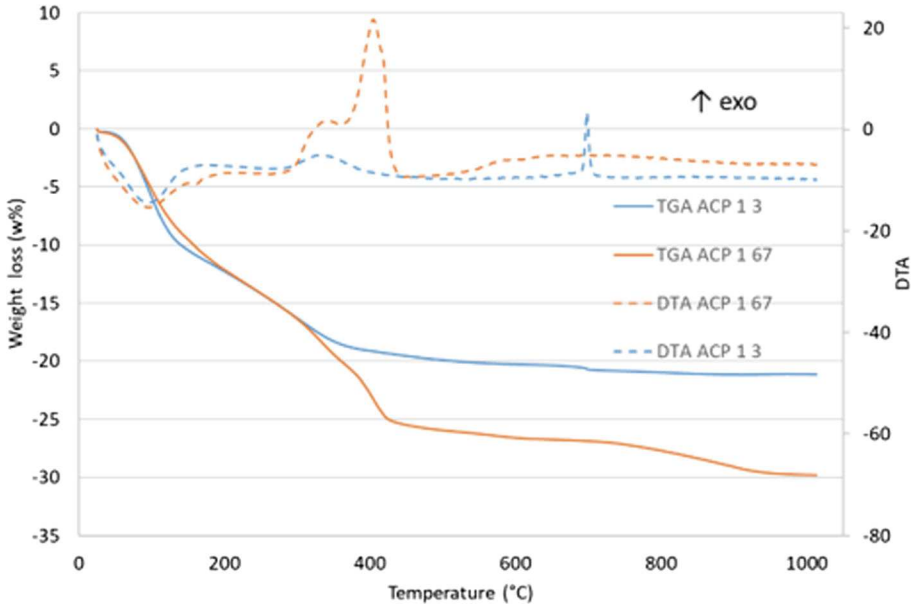

Figure 4 TGA (line) and DTA (dots) of ACP 1.67 and ACP 1.3.

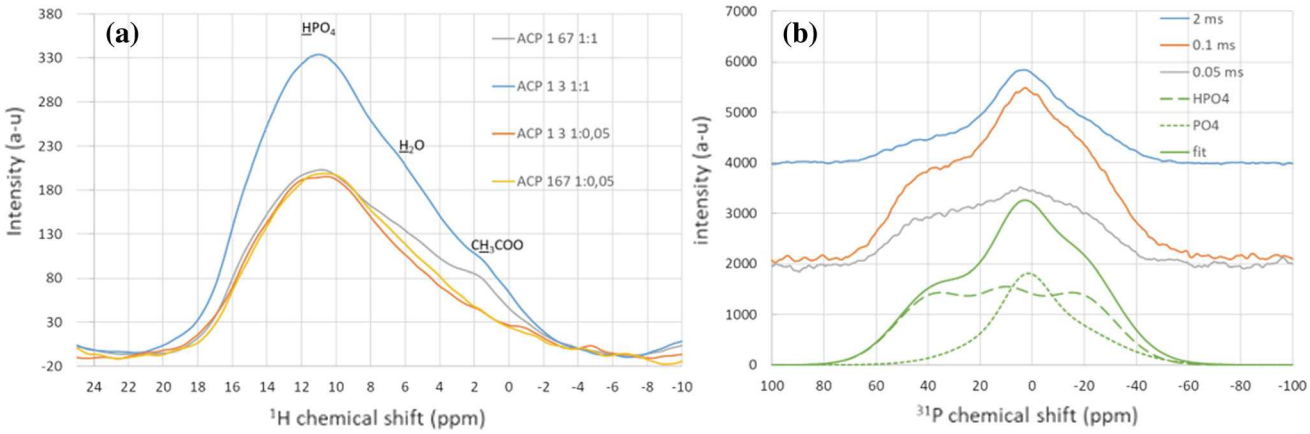

Figure 5 **a** $^{1}H/^{31}P$ DCP MAS NMR of ACP 1.67 and ACP 1.3 at 0.05 ms or 1 ms τ_2 contact time and **b** ^{31}P CP NMR in static mode with ACP 1.3 and with different contact times.

The third loss (above 400 °C) corresponds to the decomposition of the calcium carbonate resulting in reaction 2 followed by the formation of hydroxyapatite (HA) assessed by XRD data (Figure S2, Supporting Information):

$$CaCO_3 \rightarrow CaO + CO_2 \qquad \text{(reaction 3)}$$

$$CaO + 3Ca_3(PO_4)_2 + H_2O \rightarrow Ca_{10}(PO_4)_6(OH)_2 \quad \text{(reaction 4)}$$

The system is, however, complicated by the possible reaction of $CaCO_3$ with $CaHPO_4$ or $Ca_2P_2O_7$ reported in several papers [37, 38] as described in reactions 5 and 6.

$$CaCO_3 + 2CaHPO_4 \rightarrow Ca_3(PO_4)_2 + H_2O + CO_2 \quad \text{(reaction 5)}$$

$$CaCO_3 + Ca_2P_2O_7 \rightarrow Ca_3(PO_4)_2 + CO_2 \quad \text{(reaction 6)}$$

However, these reactions do not change the global weight loss of the second and third losses. Calculations were made using this sum (TGA analysis, Supplementary Information).

We can observe calcium acetate peaks at 18.4, 29.3 and 31.5° 2θ in Fig. 3 that confirm the presence of this species in the spray-dried power. These diffraction peaks correspond to the ones observed previously with SAXS. Assuming that the Ca/P ratio in the ACP 1.67 and 1.30 samples is that of the initial spray-dried solutions (no loss of Ca or P), considering the weight losses and the mass balance, it is possible to evaluate the powders composition (Table S, Supporting Information). The amount of calcium acetate much larger in the ACP 1.67 sample than in the 1.30 one is in agreement with the starting solutions compositions and the impossibility to precipitate all the calcium with phosphate ions in the ACP 1.67 sample. The excess of calcium in the ACP 1.67 sample compared to ACP 1.3 seems to induce a decrease in the proportion of HPO_4^{2-} ions in the powder and to increase the $Ca_3(PO_4)_2$ fraction.

DTA curves of both powders are slightly different. ACP 1.67 shows an endothermic broad peak corresponding to the release of water and two wide exothermic peaks corresponding to the degradation of calcium acetate, the condensation of HPO_4^{2-} in pyrophosphate and the crystallization of a poorly crystallized apatitic calcium phosphate phase. Figure S2 (Supporting Information) highlights this crystallization phenomenon for ACP 1.67 treated at 500 °C, with the appearance of diffraction peaks matching with the JCPDS # 09–0732 reference of hydroxyapatite. This poorly crystalline apatite phase then crystallized into a well-crystallized stoichiometric hydroxyapatite (Figure S2, Supporting Information). The ACP 1.3 DTA also shows the endothermic peak of water release, a small wide exothermic peak corresponding to the condensation of pyrophosphate mentioned above and a small, narrow exothermic peak at 700 °C corresponding to the crystallization of a β-TCP matching with the JCPDS # 09–0169 (Figure S2, Supporting Information). α-TCP was expected as it was obtained by

Somrani et al. heating ACP at 625 °C [39] at a rate of 10 °C.min^{-1}. Furthermore, β-TCP is a calcium phosphate with a Ca/P ratio of 1.5, whereas the Ca/P molar ratio of the initial solution was 1.3. This Ca/P molar ratio is not consistent with that of the initial composition, and the FTIR analysis (Figure S2, Supporting Information) shows, in addition to the peaks of the β-TCP phase, additional lines at 723, 753 cm^{-1} and 1000–1200 cm^{-1} characteristics of beta calcium pyrophosphate (CPP) [40]. As CPP has a Ca/P ratio of 1, it means that, to ensure the global Ca/P ratio of 1.3 of the powder (*i.e.*, the initial ratio of the solution), 60% of the powder P atoms crystallized into β-TCP and 40% reorganized into calcium pyrophosphate (molar ratios).

The ^{1}H NMR spectra obtained by a double cross polarization MAS ^{1}H → ^{31}P → ^{1}H (Fig. 5a clearly present ^{1}H resonances of HPO_4^{2-} at $\delta(^{1}H) \approx 11$ ppm regardless of the Ca/P ratio and τ_2 contact time [41]. For long τ_2 contact time (i.e., 1 ms), the $\delta(^{1}H) \approx 5.5$ ppm ^{1}H resonance characteristic of the presence of water is observed in both ACP 1.67 and ACP 1.3 samples. In addition, a ^{1}H resonance of $\delta(^{1}H) = 1.6$ ppm attributed to the proton of the acetate group is also present on the ^{1}H NMR spectra for long τ_2 contact time betraying the close proximity between the phosphate groups and the acetate ion. It can be noticed that the $\delta(^{1}H) = 1.6$ ppm contribution is more important in the ACP 1.67 sample than in the ACP 1.3. A similar result can be observed in the ^{13}C CP NMR spectra present in supplementary information (Figure S3, Supporting Information). The two peaks at $\delta(^{13}C) = 22$ ppm and around 183 ppm are characteristics of calcium acetate. In addition to the higher intensity of the ^{13}C CP spectrum of ACP 1.67, the division of the 183 ppm peak into 4 distinct peaks confirms the crystallinity of calcium acetate mentioned above. This result is to correlate with the largest amount of calcium acetate in the ACP 1.67 compared to the ACP 1.3. As the ^{1}H/^{31}P DCP MAS experiment probes the close environment of phosphorous nuclei, we can conclude that calcium acetate in excess in the precipitation reaction preferentially nucleates in the surrounding of ACP nanoparticles or cluster.

A ^{31}P MAS spectrum has been performed on the ACP 1.3 sample (Figure S4, Supporting Information), but due to the amorphous aspect of the material, the signal obtained is wide and doesn't bring much information. To overcome this issue and highlight the different phosphate species potentially present, a static CP NMR acquisition of ACP 1.3 has been performed on the powder with different contact times (i.e., 2, 0.1 and 0.05 ms) (Fig. 5b). Two types of signal can be identified: a large one assigned to the hydrogenophosphate that increases in proportion for short contact time (the ^{1}H and ^{31}P nuclei in $HPO_4^{2-}$are close to each other), and a signal corresponding to a narrower chemical shift anisotropy assigned to the PO_4^{3-} groups centered at *ca* $\delta(^{31}P) \approx 3$ ppm (the ^{31}P of PO_4^{3-} is farther from hydrogen nuclei).

Evolution of ACP 1.67 in water

As mentioned before, ACP is a transient phase that evolves in aqueous solution. A characterization of the powder evolution was monitored using granulometry, SEM images (Figure S5, Supporting Information) and XRD at different times in deionized water. In Fig. 6, it can be observed that particle size distribution rapidly evolves. In fact, a bimodal distribution appears in the first acquisition (0 s). This modification compared to the dry powder can be attributed to the beginning of the evolution of the powder in the medium. Then the population centered at 5 μm vanishes for the benefit of a population centered at 120 μm. The size distribution of the powder after 1 h is multimodal and stays constant with the main population at 110 μm and two minor populations at 18 and 450 μm. SEM images (Figure S5, Supporting Information) show an evolution of the morphology: the powder goes from spherical to plate-like shaped grain. The XRD pattern highlights this evolution with peaks corresponding to brushite $CaHPO_4{\cdot}2H_2O$ according to JCPDS # 009–0077 reference. A long-term XRD evolution is presented in Fig. 7 and shows the evolution of the resulting brushite to a poorly crystallized apatite.

Discussion

Based on these results, the spray drying of a solution made of calcium acetate and phosphoric acid precursors leads to an ACP powder. In fact, the resulting powder shows the characteristic multi-scale structure of ACP previously reported by different authors [12]: micro-size grain made of chain-like structured nanoparticles constituted of closely packed

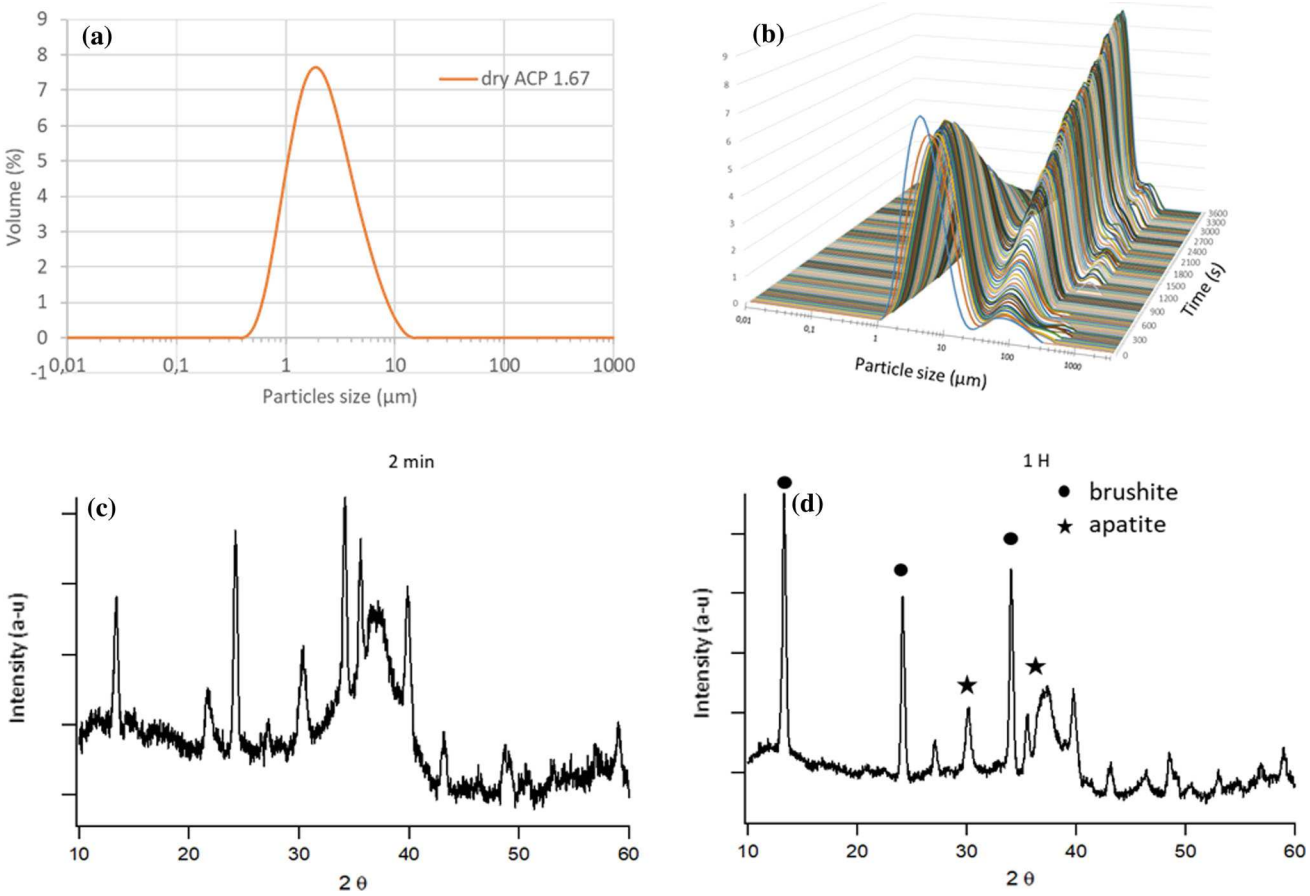

Fig. 6 **a** Dry particles size distribution of ACP 1.67, **b** evolution in aqueous solution and **c**, **d** XRD pattern after, respectively, 2 and 60 min.

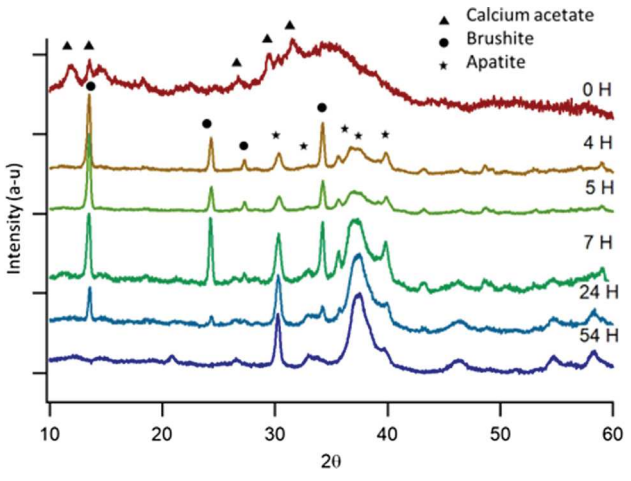

Fig. 7 Long term XRD evolution of the powder (ACP 1.67) in water, from 0 to 54 h.

nanometer clusters. These structures were reported in batch precipitation, and the fact that the identic structures are found in the spray-dried powder can point that the droplet acts as a micro-reactor. However, multiscale organization of powders can also be induced by the spray drying process itself as Sen et al. [42] mentioned. In their study, they proposed a route to explain how particles from a suspension aggregate during droplets drying, especially in the case of a «slow drying» which fit with our working conditions (i.e., diluted solution). This aggregation also leads to a multi-scale structure: nanoparticles organized in a chain-like organization and packed together to form micro-size grain. Then, it is difficult to discriminate which mechanism leads to the organization of the powder and is more probably due to a combination of both. As the presence of calcium acetate in excess in the ACP 1.67 sample is demonstrated by the different techniques used, it seems consistent that the difference in morphology between the two ACPs powders can be attributed to the amount of calcium acetate formed during drying after the precipitation of ACP. The latter could act as

a kind of surfactant or favor calcium acetate crystallization, both impacting apparent morphology/porosity of the observed aggregates.

Furthermore, the lack of long-distance organization observed in WAXS and the associated peaks width and positions are characteristics of an amorphous environment. This is confirmed by XRD broad peak around $2\theta = 35°$ (Fig. 3) and by the Raman shift of the ν_1PO_4 peak at 950 cm^{-1} (Figure S6, Supporting Information) that is characteristic of amorphous calcium phosphate [1]. This line is also present in the FTIR spectra of ACP 1.67 and ACP 1.3 (Figure S7, Supporting Information). In addition, this technique reveals characteristic intense broad lines around 1100 cm^{-1}, and 543 cm^{-1} attributed to the presence of PO_4^{3-} ions in an amorphous phases [43] and a weaker band at 870 cm^{-1} due to HPO_4^{2-} ions. Hence, spectrometric studies confirm the presence of an amorphous calcium phosphate.

However, SAXS, TGA, Raman and NMR reveal that another major compound is also present in the powder: calcium acetate. Furthermore, as the inlet spray drying temperature is 160 °C, this calcium acetate is more likely to be a semi-hydrated calcium acetate [35] as confirmed by the four peaks at 929, 951, 958 and 966 cm^{-1} characteristic of a semi-hydrated calcium acetate (Figure S2, Supporting Information). The amount of calcium acetate was determined as previously described (*Reaction 2*, Supporting Information) and is reported in Table S (Supporting Information).

Regardless of the Ca/P ratio, the morphology of ACP seems to be constant. However, an increase in the Ca/P ratio leads to more semi-hydrated calcium acetate in the resulting powder (TGA). In fact, the maximum Ca/P ratio which can be reached, with only Ca^{2+} and phosphate ions, is $Ca_3(PO_4)_2$ (Ca/P = 1.5), involving the most charged orthophosphate anion PO_4^{3-}, higher Ca/P can only be reached with additional Ca^{2+} ions and their counter ion, for example $Ca(OH)_2$ or CaF_2. In our case, it is calcium acetate mixed with ACP.

According to the $^1H/^{31}P$ DCP MAS NMR, part of acetate is close to the phosphate entities whatever the Ca/P ratio. We can hypothesize that these acetate molecules are partially organized (without crystallization) around CaP cluster as demonstrated by WAXS results for ACP 1.3. Another part of acetate is involved in a crystalline phase for ACP 1.67, as highlighted by XRD measurements. These results give a hint on the precipitation order in the drop during the drying and the powder structure formation mechanism. It implies that ACP, the most insoluble phase, first precipitates until the complete consumption of phosphorus followed by calcium acetate deposition/crystallization.

Considering SAXS results, the center-to-center distance between clusters is 2 nm. It is in contradiction with the 1 nm diameter of Posner's cluster described in the literature [13] and correlated with our present WAXS studies. Beyond uncertainties associated with respective techniques, these data suggest that Posner's clusters are not in close contact in the solids. It means that some interstitial entities may discard such clusters. As previously mentioned, acetate ions (that are not involved in calcium acetate crystals) are present in the close environment of clusters (solid state NMR). Moreover, the large amount of hydrogenophosphate (Table S, Supporting Information) in the powder may result of inter-cluster hydrated calcium hydrogenophosphate entities as described in other compounds such as crystalline triclinic octacalcium phosphate (OCP) where HPO_4^{2-} and their calcium counter ion belong to a hydrated layer [44] separating Posner's apatitic cluster or, close to our case, nanocrystalline apatite showing a hydrated layer formed mainly of HPO_4^{2-} and calcium ions on their surface [45–47]. Acetate and hydrogenophosphate could interact either with superficial Ca^{2+} that are involved in Posner's clusters and creating a layer of anions or with incorporating "free" Ca^{2+} chelated with water. These water molecules appear as essential for the solid cohesion, acting as a mortar between clusters [20, 47]. The SAXS broader and slightly more intense peak for ACP 1.67 reflects a better inter-particular arrangement. It could be correlated with the increase in acetate anions versus hydrogenophosphate anions. Indeed we could hypothesize that the length and the nature of acetate molecules lead to a better self-organization of clusters (WAXS) than hydrogenophosphate.

Based on the morphological and structural analyses, we can conclude that the powder is composed of ion clusters, with diameters of 2 nm and closely packed into nanoparticles. These nanoparticles are in turn organized in chain-like structures, and these structures then form micro-sized particles as presented in Fig. 8.

As mentioned in the introduction, ACP is a metastable material which can be rapidly altered in

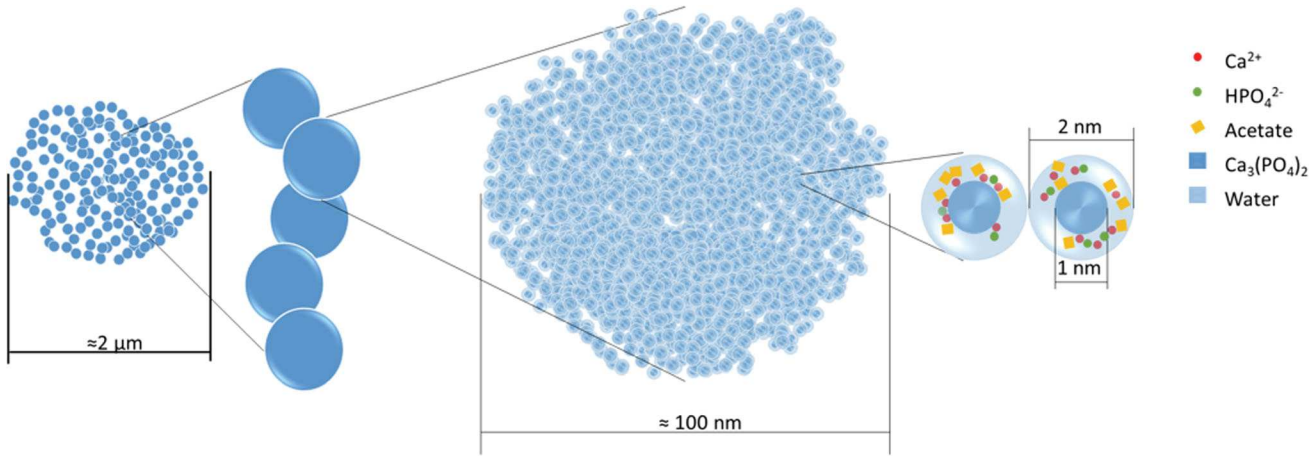

Figure 8 Schematic multi scale representation of the spray dried powder in accordance with data presented. The spray dried particles show an average size of about 2 µm, and these entities are porous and made of chain like association of spheres of about 100 nm (TEM), which are an assemblage of dense Posner's clusters ($Ca_3(PO_4)_2$ (WAXS/PDF results), surrounded by a hydrated shell of calcium hydrogen phosphate and acetate, moving apart the clusters at about 2 nm (SAXS results).

an aqueous medium or with temperature. Powders developed in this study have the ability to convert into more stable phases in aqueous solution as illustrated in Fig. 6. The size variations and crystallization process, driven by successive dissolution-reprecipitation reactions, finally lead to an apatite of low crystallinity similar to the ones observable in native bones. This kind of evolution is well known [33] and has been used in self-setting cements. In a study for instance [48], the increase in compressive strength as well as the diametral tensile strength with the increase in crystallinity of a cement is highlighted. The fact that our powder evolves first into plate-like shaped crystals (brushite) that inter-connect and then to a calcium phosphate phase similar to the one of native bone makes it a good candidate for further investigations as a calcium phosphate cement and beyond, for numerous dental and bone substitution applications [17].

Conclusion

Micrometric and structured aggregates of amorphous calcium phosphate nanoparticles have been produced by direct spray drying of a single solution of selected salt precursors. These aggregates are structured at several scale: nanometer CaP Posner's clusters are grouped in spherical nanoparticles that are organized themselves in chain-like structure. This multi-scale organization is the result of the combined effect of the fast water evaporation leading to quick and local supersaturation during the drying stage of the process.

The composition of the spray-dried ACP may be modulated by tailoring the initial composition of the precursors solution, both formulations tested (1.67 and 1.3). Beyond calcium and phosphate ions that are involved in the core of clusters, acetate and hydrogenophosphate anions and water play a key role in the structuration of inter-cluster spaces, leading to the final cohesion of the material. Moreover, the proportion of acetate and hydrogenophosphate can be tuned by the initial Ca/P ratio. Lower hydrogenophosphate amounts induce a better arrangement between clusters.

Initial undersaturated condition prevents early precipitation before spray drying and allows to generate due to the high drying rate of the process a highly reactive powder. Their high HPO_4 content confers strong ability to spontaneously evolve in aqueous medium to form a dicalcium phosphate dihydrate phase that evolves into biomimetic apatite

Regarding calcium acetate impurities and biocompatibility, a study has reported good results of implantations in rats of PPF (polypropylene glycol-co-fumaric acid) cements with this additive [49, 50]. It shall be considered that the technique can be adapted to control this residue.

These findings demonstrate the suitability of our spray-drying-derived process to produce a metastable and reactive powder by a simple and

quick method, opening the way for the development of materials for biomedical applications and especially as bone and dental substitutes. Indeed, such spray-dried ACP obtained with well-defined size powder appears to be promising product with enhanced handling properties compared to large and coarse distribution usually derived from co-precipitation route, maintaining the scalability of this process for further industrialization.

Acknowledgements

The authors would like to acknowledge Marianne Clerc-Imperor for helpful discussions about SAXS results, Gwénaëlle Guittier (LGC) for N2 adsorption measurements and Cédric Charvillat (CIRIMAT) for XRD and TGA-TDA measurements. They also want to thank Alessandro Pugliara and Teresa Hungria (Centre de MicroCaractérisation Raimond Castaing UMS 3623) and Stéphanie Balor (METi) for the TEM analyses. The FERMaT Federation FR3089, Université de Toulouse, CNRS, is acknowledged too for providing small-angle X-ray scattering laboratory facility.

Electronic supplementary material: The online version of this article (https://doi.org/10.1007/s10853-020-05396-7) contains supplementary material, which is available to authorized users.

References

[1] Kazanci M, Fratzl P, Klaushofer K, Paschalis EP (2006) Complementary information on in vitro conversion of amorphous (precursor) calcium phosphate to hydroxyapatite from Raman microspectroscopy and wide angle X ray scattering. Calcif Tissue Int 79:354 359. https://doi.org/10.1007/s00223 006 0011 9

[2] Lotsari A, Rajasekharan AK, Halvarsson M, Andersson M (2018) Transformation of amorphous calcium phosphate to bone like apatite. Nat Commun 9(1):1 11. https://doi.org/10.1038/s41467 018 06570 x

[3] Dey A, Bomans PHH, Müller FA et al (2010) The role of prenucleation clusters in surface induced calcium phosphate crystallization. Nat Mater 9:1010 1014. https://doi.org/10.1038/nmat2900

[4] Ridi F, Meazzini I, Castroflorio B et al (2017) Functional calcium phosphate composites in nanomedicine. Adv Colloid Interface Sci 244:281 295. https://doi.org/10.1016/j.cis.2016.03.006

[5] Mahamid J, Sharir A, Addadi L, Weiner S (2008) Amorphous calcium phosphate is a major component of the forming fin bones of zebrafish: indications for an amorphous precursor phase. Proc Natl Acad Sci 105:12748 12753. https://doi.org/10.1073/pnas.0803354105

[6] Mahamid J, Aichmayer B, Shimoni E et al (2010) Mapping amorphous calcium phosphate transformation into crystalline mineral from the cell to the bone in zebrafish fin rays. Proc Natl Acad Sci 107:6316 6321. https://doi.org/10.1073/pnas.0914218107

[7] Samavedi S, Whittington AR, Goldstein AS (2013) Calcium phosphate ceramics in bone tissue engineering: a review of properties and their influence on cell behavior. Acta Biomater 9:8037 8045. https://doi.org/10.1016/j.actbio.2013.06.014

[8] Dorozhkin SV (2009) Calcium orthophosphate cements and concretes. Materials 2(1):221 291. https://doi.org/10.3390/ma2010221

[9] Skrtic D, Antonucci JM, Eanes ED (2003) Amorphous calcium phosphate based bioactive polymeric composites for mineralized tissue regeneration. J Res Natl Inst Stand Technol 108:167 182. https://doi.org/10.6028/jres.108.017

[10] Zhao J, Liu Y, Bin SW, Yang X (2012) First detection, characterization, and application of amorphous calcium phosphate in dentistry. J Dent Sci 7:316 323. https://doi.org/10.1016/j.jds.2012.09.001

[11] Brečević L, Hlady V, Füredi Milhofer H (1987) Influence of gelatin on the precipitation of amorphous calcium phosphate. Colloids Surf 28:301 313. https://doi.org/10.1016/0166 6622(87)80191 9

[12] Habraken WJEM, Tao J, Brylka LJ et al (2013) Ion association complexes unite classical and non classical theories for the biomimetic nucleation of calcium phosphate. Nat Commun 4:1507 1512. https://doi.org/10.1038/ncomms2490

[13] Betts F, Posner AS (1974) An X ray radial distribution study of amorphous calcium phosphate. Mater Res Bull 9:353 360. https://doi.org/10.1016/0025 5408(74)90087 7

[14] Onuma K, Ito A (1998) Cluster growth model for hydroxyapatite. Chem Mater 10:3346 3351. https://doi.org/10.1021/cm980062c

[15] Termine JD, Eanes ED (1972) Comparative chemistry of amorphous and apatitic calcium phosphate preparations. Calcif Tissue Res 10:171 197. https://doi.org/10.1007/BF02012548

[16] Dorozhkin SV (2009) Calcium orthophosphates in nature, biology and medicine. Materials (Basel) 2:399 498. https://doi.org/10.3390/ma2020399

[17] Combes C, Rey C (2010) Amorphous calcium phosphates: synthesis, properties and uses in biomaterials. Acta Biomater 6:3362 3378. https://doi.org/10.1016/j.actbio.2010.02.017
[18] Baig AA, Fox JL, Young RA et al (1999) Relationships among carbonated apatite solubility, crystallite size, and microstrain parameters. Calcif Tissue Int 64:437 449. https://doi.org/10.1007/PL00005826
[19] Bussola Tovani C, Gloter A, Azaïs T et al (2019) Formation of stable strontium rich amorphous calcium phosphate: possible effects on bone mineral. Acta Biomater 92:315 324. https://doi.org/10.1016/j.actbio.2019.05.036
[20] Mayen L, Jensen ND, Laurencin D et al (2020) A soft chemistry approach to the synthesis of amorphous calcium ortho/pyrophosphate biomaterials of tunable composition. Acta Biomater 103:333 345. https://doi.org/10.1016/j.actbio.2019.12.027
[21] Ortali C, Julien I, Vandenhende M et al (2018) Consolidation of bone like apatite bioceramics by spark plasma sintering of amorphous carbonated calcium phosphate at very low temperature. J Eur Ceram Soc 38:2098 2109. https://doi.org/10.1016/j.jeurceramsoc.2017.11.051
[22] Uskoković V, Marković S, Veselinović L et al (2018) Insights into the kinetics of thermally induced crystallization of amorphous calcium phosphate. Phys Chem Chem Phys 20:29221 29235. https://doi.org/10.1039/c8cp06460a
[23] Eanes ED, Posner AS (1965) Division of biophysics: kinetics and mechanism of conversion of noncrystalline calcium phosphate to crystalline hydroxyapatite. Trans N Y Acad Sci 28:233 241. https://doi.org/10.1111/j.2164 0947.1965.tb02877.x
[24] Chow LC, Sun L, Hockey B (2004) Properties of nanostructured hydroxyapatite prepared by a spray drying technique. J Res Natl Inst Stand Technol 109:543 551. https://doi.org/10.6028/jres.109.041
[25] Xu HHK, Moreau JL, Sun L, Chow LC (2011) Nanocomposite containing amorphous calcium phosphate nanoparticles for caries inhibition. Dent Mater 27:762 769. https://doi.org/10.1016/j.dental.2011.03.016
[26] Melo MAS, Weir MD, Passos VF et al (2017) Ph activated nano amorphous calcium phosphate based cement to reduce dental enamel demineralization. Artif Cells Nanomedicine Biotechnol 45:1778 1785. https://doi.org/10.1080/21691401.2017.1290644
[27] Sun L, Chow LC, Frukhtbeyn SA, Bonevich JE (2010) Preparation and properties of nanoparticles of calcium phosphates with various Ca/P ratios. J Res Natl Inst Stand Technol 115:243 255. https://doi.org/10.6028/jres.115.018
[28] Safronova TV, Mukhin EA, Putlyaev VI et al (2017) Amorphous calcium phosphate powder synthesized from calcium acetate and polyphosphoric acid for bioceramics application. Ceram Int 43:1310 1317. https://doi.org/10.1016/j.ceramint.2016.10.085
[29] Hammouda B, Ho DL, Kline S (2004) Insight into clustering in poly(ethylene oxide) solutions. Macromolecules 37:6932 6937. https://doi.org/10.1021/ma049623d
[30] Zernike F, Prins JA (1927) Die Beugung von Röntgen strahlen in Flüssigkeiten als Effekt der Molekülanordnung. Zeitschrift für Phys 41:184 194. https://doi.org/10.1007/BF01391926
[31] Dassenoy F, Philippot K, Ould Ely T et al (1998) Platinum nanoparticles stabilized by CO and octanethiol ligands or polymers: FT IR, NMR, HREM and WAXS studies. New J Chem 22:703 711. https://doi.org/10.1039/a709245h
[32] Von Euw S, Ajili W, Chan Chang THC et al (2017) Amorphous surface layer versus transient amorphous precursor phase in bone a case study investigated by solid state NMR spectroscopy. Acta Biomater 59:351 360. https://doi.org/10.1016/j.actbio.2017.06.040
[33] Kim S, Ryu HS, Shin H et al (2005) In situ observation of hydroxyapatite nanocrystal formation from amorphous calcium phosphate in calcium rich solutions. Mater Chem Phys 91:500 506. https://doi.org/10.1016/j.matchemphys.2004.12.016
[34] Brečević L, Füredi Milhofer H (1972) Precipitation of calcium phosphates from electrolyte solutions. Calcif Tissue Res 10:82 90. https://doi.org/10.1007/BF02012538
[35] Saury C, Boistelle R, Dalemat F, Bruggeman J (1993) Solubilities of calcium acetates in the temperature range 0 100 °C. J Chem Eng Data 38:56 59. https://doi.org/10.1021/je00009a013
[36] Judd MD, Plunkett BA, Pope MI (1974) The thermal decomposition of calcium, sodium, silver and copper(II) acetates. J Therm Anal 6:555 563. https://doi.org/10.1007/BF01911560
[37] Famery R, Richard N, Boch P (1994) Preparation of α and β tricalcium phosphate ceramics, with and without magnesium addition. Ceram Int 20:327 336. https://doi.org/10.1016/0272 8842(94)90050 7
[38] Durucan C, Brown PW (2002) Reactivity of α tricalcium phosphate. J Mater Sci 37:963 969. https://doi.org/10.1023/A:1014347814241
[39] Somrani S, Rey C, Jemal M (2003) Thermal evolution of amorphous tricalcium phosphate. J Mater Chem 13(4):888 892. https://doi.org/10.1039/b210900j
[40] Gras P, Teychené S, Rey C et al (2013) Crystallisation of a highly metastable hydrated calcium pyrophosphate phase. Cryst Eng Comm 15:2294 2300. https://doi.org/10.1039/c2ce26499d
[41] Tseng YH, Zhan J, Lin KSK et al (2004) High resolution 31P NMR study of octacalcium phosphate. Solid State Nucl

Magn Reson 26:99 104. https://doi.org/10.1016/j.ssnmr.2004.06.002

[42] Sen D, Spalla O, Taché O et al (2007) Slow drying of a spray of nanoparticles dispersion. In situ SAXS investigation. Langmuir 23:4296 4302. https://doi.org/10.1021/la063245j

[43] Stutman JM, Termine JD, Posner AS (1965) Vibrational spectra and structure of the phosphate ion in some calcium phosphates. Trans N Y Acad Sci 27:669 675. https://doi.org/10.1111/j.2164 0947.1965.tb02224.x

[44] Mathew M, Brown WE, Schroeder LW, Dickens B (1988) Crystal structure of octacalcium bis(hydrogenphosphate) tetrakis(phosphate)pentahydrate, Ca8(HP04)2(PO4)4·5H2O. J Crystallogr Spectrosc Res 18:235 250. https://doi.org/10.1007/BF01194315

[45] Vandecandelaere N, Rey C, Drouet C (2012) Biomimetic apatite based biomaterials: on the critical impact of synthesis and post synthesis parameters. J Mater Sci Mater Med 23:2593 2606. https://doi.org/10.1007/s10856 012 4719 y

[46] Von Euw S, Wang Y, Laurent G et al (2019) Bone mineral: new insights into its chemical composition. Sci Rep 9:1 11. https://doi.org/10.1038/s41598 019 44620 6

[47] Duer M, Veis A (2013) Water brings order. Nat Mater 12:1081 1082. https://doi.org/10.1038/nmat3822

[48] Wang X, Ye J, Wang Y et al (2007) Control of crystallinity of hydrated products in a calcium phosphate bone cement. J Biomed Mater Res Part A 81:781 790. https://doi.org/10.1002/jbm.a.31059

[49] Tsukeoka T, Suzuki M, Ohtsuki C et al (2006) Mechanical and histological evaluation of a PMMA based bone cement modified with γ methacryloxypropyltrimethoxysilane and calcium acetate. Biomaterials 27:3897 3903. https://doi.org/10.1016/j.biomaterials.2006.03.002

[50] Lewandrowski KU, Gresser JD, Wise DL, Trantolo DJ (2000) Bioresorbable bone graft substitutes of different osteoconductivities: a histologic evaluation of osteointegration of poly(propylene glycol co fumaric acid) based cement implants in rats. Biomaterials 21:757 764. https://doi.org/10.1016/S0142 9612(99)00179 9